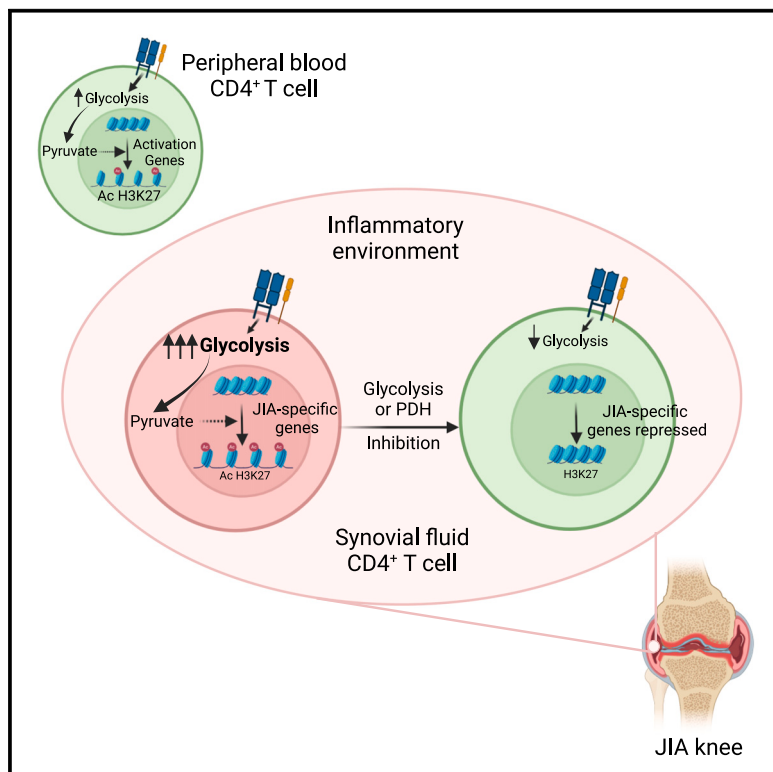


Glycolytic reprogramming shapes the histone acetylation profile of activated CD4⁺ T cells in juvenile idiopathic arthritis

Graphical abstract



Authors

Enric Mocholi, Edward Corrigan,
Theo Chalkiadakis, ...,
Jorg van Loosdregt, Stefan Prekovic,
Paul J. Coffer

Correspondence

emocholi@uchceu.es (E.M.),
pcoffer@umcutrecht.nl (P.J.C.)

In brief

Juvenile idiopathic arthritis (JIA) is an autoimmune disorder characterized by CD4⁺ T cell accumulation in synovial fluid (SF). Mocholi et al. identify glycolysis as key player in driving disease-specific H3K27acetylation and transcription in JIA CD4⁺ T cells. Targeting glycolysis or PDH reverses JIA-associated gene expression changes, offering therapeutic potential.

Highlights

- JIA CD4⁺ T cells show increased glycolysis, driving transcriptional reprogramming
- Heightened H3K27ac at JIA-associated genes connects metabolism to epigenetic control
- Inhibiting glycolysis or PDH reduces H3K27ac, highlighting potential treatment options



Article

Glycolytic reprogramming shapes the histone acetylation profile of activated CD4⁺ T cells in juvenile idiopathic arthritis

Enric Mocholi,^{1,2,5,*} Edward Corrigan,^{1,2} Theo Chalkiadakis,¹ Can Gulersonmez,¹ Edwin Stigter,¹ Bas Vastert,^{3,4} Jorg van Loosdregt,³ Stefan Prekovic,¹ and Paul J. Coffer^{1,2,3,6,*}

¹Center for Molecular Medicine, University Medical Center Utrecht, Utrecht, the Netherlands

²Regenerative Medicine Center, University Medical Center Utrecht, Utrecht, the Netherlands

³Center for Translational Immunology, University Medical Center Utrecht, Utrecht, the Netherlands

⁴Division of Pediatrics, University Medical Center Utrecht, Utrecht, the Netherlands

⁵Present address: Departamento Ciencias Biomédicas, Universidad Cardenal Herrera CEU, Valencia, Spain

⁶Lead contact

*Correspondence: emocholi@uchceu.es (E.M.), pcoffer@umcutrecht.nl (P.J.C.)

<https://doi.org/10.1016/j.celrep.2025.115287>

SUMMARY

Juvenile idiopathic arthritis (JIA) is an autoimmune disease characterized by accumulation of activated CD4⁺ T cells in the synovial fluid (SF) of affected joints. JIA CD4⁺ T cells exhibit a unique inflammation-associated epigenomic signature, but the underlying mechanisms remain unclear. We demonstrate that CD4⁺ T cells from JIA SF display heightened glycolysis upon activation and JIA-specific H3K27 acetylation, driving transcriptional reprogramming. Pharmacological inhibition of glycolysis altered the expression of genes associated with these acetylated regions. Healthy CD4⁺ T cells exposed to JIA SF exhibited increased glycolytic activity and transcriptomic changes marked by heightened histone 3 lysine 27 acetylation (H3K27ac) at JIA-specific genes. Elevated H3K27ac was dependent on glycolytic flux, while inhibiting glycolysis or pyruvate dehydrogenase (PDH) impaired transcription of SF-driven genes. These findings demonstrate a key role of glycolysis in JIA-specific gene expression, offering potential therapeutic targets for modulating inflammation in JIA.

INTRODUCTION

Juvenile idiopathic arthritis (JIA) is a heterogeneous group of autoimmune conditions characterized by chronic arthritis with an unknown cause and onset before the age of 16 years. It is marked by the accumulation of mononuclear cell populations, notably including activated CD4⁺ memory/effector T (T_{mem}/T_{eff}) cells, within the synovial fluid of afflicted joints.¹ The pivotal role of T_{mem}/T_{eff} cells in the pathophysiology of JIA has been well established.² JIA is a relevant model for the exploration of autoimmune pathogenesis, primarily due to its early onset and the potential for in-depth analysis of immune cells derived from inflamed anatomical sites. Previously, we identified a unique disease-specific epigenomic signature (in this paper, the term “epigenome” refers specifically to histone acetylation that can influence gene expression) linked to inflammation in CD4⁺ T cells isolated from the synovial fluid of patients with JIA.³ However, the molecular mechanisms underlying epigenome dysregulation in JIA T cells, or T cells associated with other autoinflammatory conditions, remain unclear.

Intracellular metabolism is critical in modulating immune activation, influencing fundamental processes such as proliferation, differentiation, cell fate, and functions.⁴ Upon activation of the T cell receptor (TCR), a metabolic program is initiated that not only en-

hances mitochondrial function but also engages aerobic glycolysis.⁴ Recent studies have identified an essential role of glycolysis in orchestrating epigenetic and transcriptional changes during T cell activation and differentiation.^{5–8} However, it remains unclear how this is impacted when considering inflammatory environments. Initial investigations in individuals with rheumatoid arthritis (RA) have delineated a disease-specific metabolic signature.⁹ This underlies the transformation of naive CD4⁺ T cells into pro-inflammatory helper T cells, which subsequently infiltrate joints and provoke inflammation through immunogenic cell death.¹⁰ These pro-inflammatory T cells infiltrate the RA synovium, contributing to tissue damage.¹¹ Activated RA T cells are unable to upregulate expression of the key glycolytic enzyme 6-phosphofructo-2-kinase/fructose-2,6-bisphosphatase 3 (PFKFB3), an indication that patient-derived cells utilize glucose differently.¹² In a human tissue-mouse chimera model, selective knockdown of PFKFB3 in adoptively transferred healthy T cells was sufficient to induce robust synovial inflammation, generating a transcriptome pattern reminiscent of rheumatoid synovitis.¹³ Conversely, the rescue of PFKFB3 expression in adoptively transferred RA T cells was effective in dampening synovial tissue inflammation. In essence, by shifting the ratio of PFKFB3/G6PD (glucose-6-phosphate-dehydrogenase), RA T cells divert glucose from ATP production toward



biosynthesis, generating inflammation-inducing effector cells. Furthermore, mitochondrial oxygen consumption is significantly suppressed in RA T cells despite mitochondrial mass being comparable to that in healthy T cells.¹⁴ A better understanding of the role of metabolic signals in T cell specification opens the possibility for immunomodulation before the end stage of synovial inflammation encountered in clinical practice.⁹

Methotrexate, which inhibits dihydrofolate reductase, is a first-line treatment for many patients with RA. Notably, methotrexate has been shown to significantly reduce the expression of hexokinase II and glucose/fructose transporters, such as SLC2A5, a member of the solute carrier family 2. This suggests that methotrexate can modulate glycolytic activity, further highlighting its role in altering metabolic pathways in RA therapy.¹⁵ Pre-clinical studies have also demonstrated that inhibiting mechanistic target of rapamycin (mTOR), a key regulator of metabolism, particularly glycolysis, by using rapamycin may offer therapeutic benefits in treating RA. This approach targets the reduction of fibroblast-like synoviocyte-mediated joint injury and erosive damage. Furthermore, combining mTOR inhibitors with vitamin D3 has been shown to prevent bone destruction in RA.^{16,17}

Metabolic changes in synovial fluid (SF)-resident immune cells present potential therapeutic targets, making targeting intracellular metabolism a promising avenue for disease modulation. Here, we examined the interplay between metabolic reprogramming and epigenetic regulation in controlling CD4⁺ T cell activation in JIA. T cells from the SF of individuals with JIA display anomalous intracellular metabolism and epigenetic profiles. Inhibiting glycolytic flux affected the expression of genes associated with this aberrant epigenetic profile. Furthermore, SF has the capacity to activate acetylation promoters normally associated with pathogenic JIA T cells. These changes in the epigenetic profile are contingent upon glycolysis-derived acetyl-coenzyme A (CoA) production facilitated by pyruvate dehydrogenase. This underscores the close connection between glycolysis, transcriptional responses, and T cell functionality. Understanding the impact of metabolic changes in pathological settings provides a foundation for developing therapeutic interventions aimed at selectively targeting these pathways.

RESULTS

SF JIA T cells are metabolically reprogrammed with increased activation-induced glycolysis

To evaluate the effect of local inflammation on CD4⁺ T cell metabolic responses, we conducted an analysis of intermediate metabolites associated with glycolysis and the Tricarboxylic Acid (TCA) cycle. Specifically, we compared the levels of these metabolites in CD4⁺ T cells derived from the SF of patients with active JIA to those from healthy controls obtained from peripheral blood (PB HC CD4⁺). CD4⁺ T cells were polyclonally activated with anti-CD3/CD28 in the presence of D-glucose-¹³C₆. We subsequently measured the levels of intracellular ¹³C-labeled intermediate metabolites associated with glycolysis and TCA by liquid chromatography (LC)-mass spectrometry (MS) (Figure 1A). Increased concentrations of intermediary metabolites linked to glycolysis and the TCA cycle in SF JIA T cells and PB HC T cells were observed.

To further investigate the glycolytic responses of PB HC CD4⁺, PB JIA CD4⁺, and SF JIA CD4⁺ T cells, we performed *in vitro* activation using anti-CD3/CD28 for 24 h and assessed mitochondrial respiration and aerobic glycolysis through measurements of the Oxygen Consumption Rate (OCR) and extracellular acidification rate (ECAR), respectively. We did not observe significant differences in mitochondrial respiration (Figure 1B), ATP production by mitochondria (Figures S1A and S1B, or maximal respiration levels (Figure 1C). However, basal glycolysis was markedly increased in JIA SF CD4⁺ T cells following T cell activation compared to HCs and CD4⁺ T cells isolated from the PB of the same patients with JIA (Figures 1D and 1E). These cells also exhibited changes in glycolytic capacity and glycolytic reserve (Figures S1C and S1D), but these differences were not statistically significant.

Glycolytic flux can directly reprogram the epigenetic landscape, as exemplified, for example, by increased histone acetylation.¹⁸ We measured the intracellular levels of acetyl-CoA in JIA CD4⁺ T cells isolated from both the PB and SF either in a resting state or when stimulated with anti-CD3/CD28 for 24 h. CD3/CD28-mediated activation induced an increase in intracellular acetyl-CoA levels, but the increase was significantly higher in JIA SF CD4⁺ T cells (Figure 1F).

Taken together, SF JIA T cells exhibit changes in intracellular metabolism marked by elevated activation-induced levels of TCA and glycolytic intermediate metabolites. This metabolic dysregulation is concomitant with increased glycolytic flux and acetyl-CoA production upon activation.

JIA CD4⁺ T cells exhibit an abnormal activation-induced H3K27ac landscape

To gain further insights into epigenetic and transcriptomic reprogramming occurring during the activation of SF JIA CD4⁺ T cells, we conducted chromatin immunoprecipitation sequencing (ChIP-seq) experiments targeting histone 3 lysine 27 acetylation (H3K27ac), a histone modification associated with acetylated regions.¹⁹ To this end, we isolated CD4⁺ T cells from both PB HC and SF from patients with JIA. These cells were cultured *in vitro* under resting conditions for 24 h to minimize the direct impact of the synovial inflammatory milieu. Subsequently, cells were stimulated with anti-CD3/CD28 for 24 h (Figure 2A). Significant differences were observed in the H3K27ac profiles of CD4⁺ T cells isolated from SF JIA compared to those from HCs. JIA T cells exhibited over 6,000 regions with increased acetylation, while more than 5,000 regions lost acetylation compared to the HC group. Further evaluation using Gene Ontology (GO) term analysis highlighted that regions that were more acetylated on the JIA CD4⁺ T cells were associated with genes involved in T cell activation, differentiation, proliferation, and cytokine production (Figures 2B and S1E). These findings demonstrate distinct activation-induced H3K27ac profiles in SF JIA T cells compared to PB HCs. Additionally, using gene set enrichment analysis (GSEA), we observed a robust correlation between genes exhibiting increased H3K27 acetylation in JIA T cells and those undergoing upregulation upon T cell activation (Figure S1F). Furthermore, there was a significant association between increased H3K27ac (within 5 kb of the transcription start site) in SF JIA T cells and genes linked to crucial immune

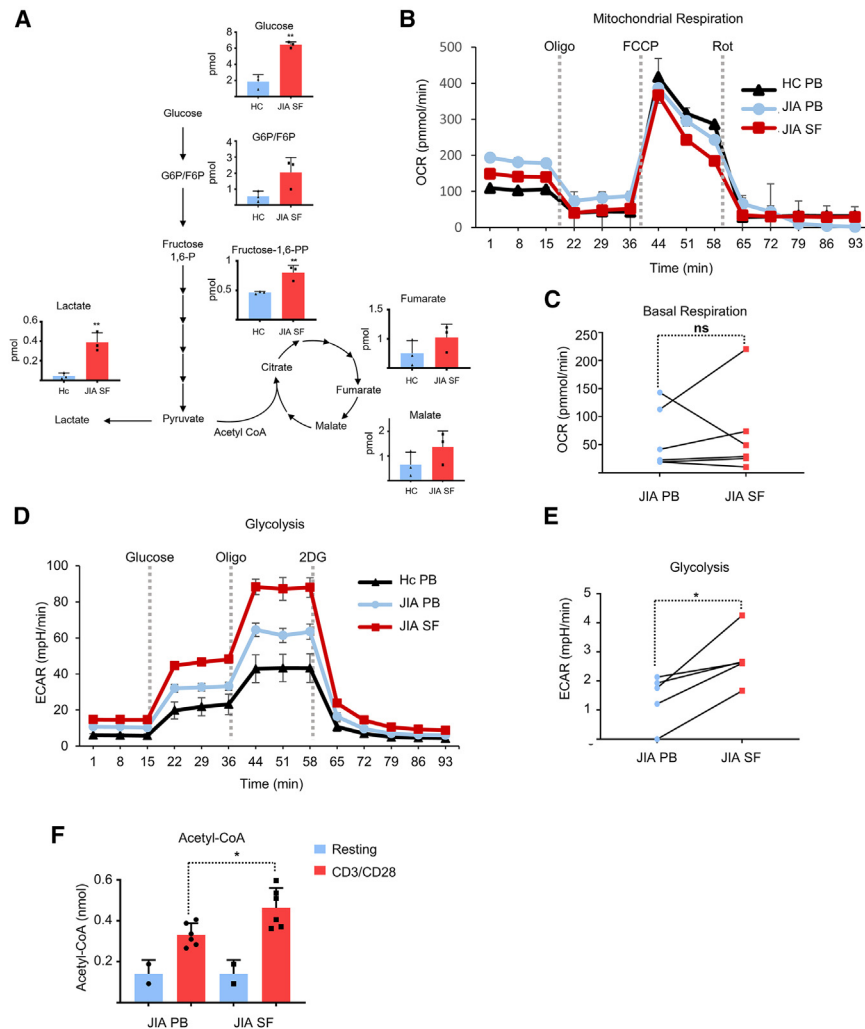


Figure 1. Enhanced activation-induced glycolysis in SF JIA CD4⁺ T cells

(A) HC PB or JIA SF CD4⁺ T cells were activated for 24 h with anti-CD3/CD28. Cell lysates from 3 biological replicates were extracted and analyzed using high-resolution liquid chromatography-Q exactive mass spectrometry to determine cellular metabolites. A representation of relative levels of metabolites in the glycolysis and TCA cycle pathways is shown. Data are shown as mean \pm SD of triplicate samples.

(B and C) JIA from PB or SF CD4⁺ T cells was activated for 24 h with CD3/CD28, and oxygen consumption rates (OCRs) were measured by Seahorse technology.

(D and E) JIA from PB or SF CD4⁺ T cells was activated for 24 h with CD3/CD28, and extracellular acidification rates (ECARs) were measured by Seahorse technology.

(F) HC PB or JIA SF CD4⁺ T cells isolated were activated for 24 h with anti-CD3/CD28, and acetyl-CoA levels were measured.

All graphs represent mean \pm SD. One-way ANOVA or paired Student's t test measured statistical significance. * $p < 0.05$, ** $p < 0.01$.

CD4⁺ T cells in contrast to PB HC T cells (Figures 2G, S1H, and S1I). To validate the relevance of these H3K27ac regions, we measured the expression levels of *IL10RA*, *TRPS1*, *PNRC1*, *CD74*, and *CD80* upon *in vitro* activation of SF JIA T cells. We indeed observed significant upregulation of these genes in SF JIA T cells compared to PB HC T cells (Figure 2H). These data substantiate the correlation between the aberrant epigenome of these cells and their transcriptome.

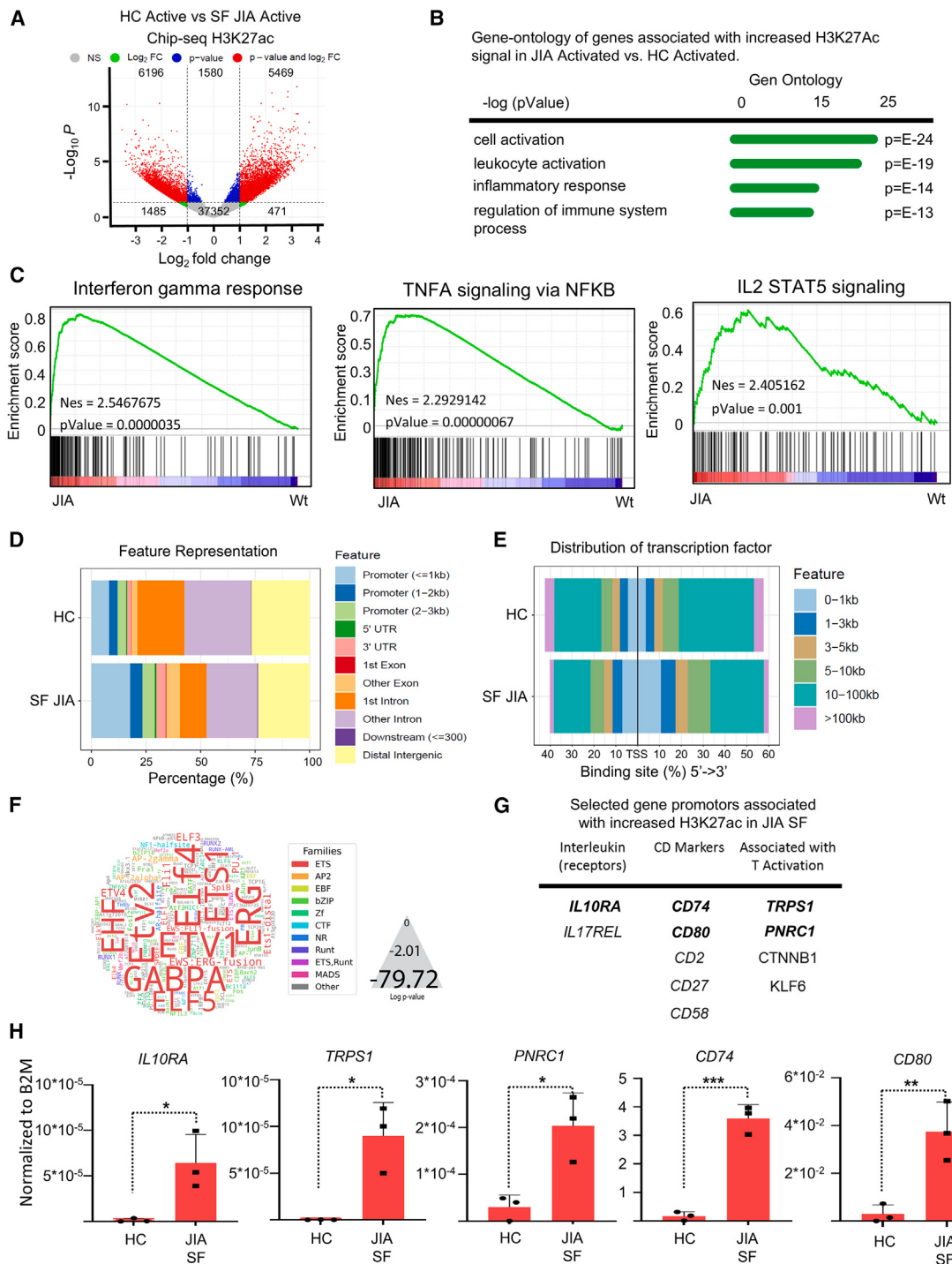
Collectively, these results indicate that T cells isolated from the SF of patients with JIA maintain an aberrant epigenome even upon *ex vivo* activation. Notably, there is increased accessibility in the promoter regions of multiple genes involved in immune effector pathways.

JIA SF drives metabolic reprogramming and a dysregulated H3K27ac landscape

To further investigate the potential link between the metabolic dysregulation observed in SF JIA CD4⁺ T cells and their aberrant H3K27ac profile, HC CD4⁺ T cells were activated *in vitro* with anti-CD3/CD28 for 24 h in the presence of either 30% SF or 30% plasma from patients with JIA. Using Seahorse metabolic profiling, we evaluated changes in OCR and ECAR as indicators of mitochondrial respiration and aerobic glycolysis, respectively. SF did not significantly impact the OCR of T cells compared to plasma from the same patients (Figures 3A, 3B, S2A, and S2B). However, CD4⁺ T cells stimulated in the presence of SF displayed a significant elevation in glycolysis, glycolytic reserve, and glycolytic capacity compared to those activated in the presence of plasma derived from the same individuals (Figures 3C, 3D, S2C,

effector pathways such as interferon gamma response, tumor necrosis factor alpha (TNF- α) signaling via nuclear factor κ B (NF- κ B), and interleukin-2 (IL-2)-STAT5 signaling (Figure 2C). Approximately one-third of the annotated peaks, upregulated in SF JIA T cells compared to HC T cells, were found to localize to promoter regions (Figure 2D). This observation was further supported by analysis of transcription factor binding sites, where >25% are in proximity (<5 kb) to H3K27ac peaks (Figure 2E). When comparing transcription factor binding profiles between SF JIA and HC T cells, both groups demonstrated enrichment for transcription factors in the E26 transformation-specific (ETS) family (Figures 2F and S1G). Notably, HC T cells exhibited additional enrichment for transcription factors from the basic-helix-loop-helix (bHLH), AP2/ethylene-responsive element binding protein, myeloblastosis (MYB)-related, and zinc finger (Zf) families (Figure S1G), while SF JIA T cells showed strong enrichment in ETS family members along with transcription factors from the AP2 and EBF families (Figure 2F).

Through a comprehensive comparison of H3K27ac datasets between HCs and SF JIA, we successfully identified specific disease-related promoters that exhibited upregulation in SF JIA



and S2D). These findings resemble the data of SF-activated CD4⁺ T cells (Figures 1D and 1E), underscoring the distinctive metabolic profile of JIA SF and suggesting a potential role for SF in enhancing glycolytic pathways and fueling their effector functions.

We next investigated the effects of SF on the transcriptome of HC CD4⁺ T cells. PB HC CD4⁺ T cells rested or were activated with anti-CD3/CD28 for 24 h in the presence of either 30% SF or 30% plasma from patients with JIA. Changes in the CD4⁺ T cell transcriptome induced by SF were evaluated by RNA sequencing (RNA-seq) analysis. SF was found to upregulate expression of genes associated with immune responses, while in activated cells, it enhanced the expression of genes involved in T cell activation pathways, including those related to G-protein signaling and calcium channels (Figures 3E, 3F, S2E, and S2F). To further examine the impact of SF on H3K27ac modifications at acetylated regions upregulated in JIA SF CD4⁺ T cells, PB HC CD4⁺ T cells were activated under similar conditions. H3K27ac ChIP-qPCR analysis was employed to quantify the acetylation levels of promoters associated with the genes *IL10RA*, *TRPS1*, *PNRC1*, *CD74*, and *CD80* (Figure 3G). Notably, CD4⁺ T cells activated in the presence of SF exhibited a significant increase in H3K27ac at these JIA-associated promoters compared to cells treated with matched plasma.

The SF composition of patients with JIA is highly complex and has been shown previously to contain elevated levels of TNF- α and IL-6.²⁰ To determine whether TNF- α or IL-6 plays a role in the induction of glycolysis and gene expression changes in T cells exposed to JIA SF, we activated T cells in the presence of SF along with anti-TNF α blocking antibodies (adalimumab [ADA] or etanercept [ENT]) or anti-IL6 blocking antibody (Tocilizumab [TCZ]). Using Seahorse analysis, we measured the ECAR as an indicator of aerobic glycolysis. Blocking antibodies against TNF- α or IL-6 did not significantly alter the glycolysis rate in T cells activated in the presence of SF (Figures S3A and S3B). To determine whether inhibition of TNF- α or IL-6 affects H3K27ac modifications at acetylated regions specifically upregulated by JIA SF in CD4⁺ T cells, we activated PB CD4⁺ T cells from HCs with anti-CD3/CD28 for 24 h in the presence of 30% JIA SF and either anti-TNF- α (ADA or ENT) or anti-IL6 (TLI2) blocking antibodies. We then measured the mRNA expression levels of *TRPS1*, *PNRC1*, *CD74*, and *CD80* by RT-qPCR. Consistent with the glycolysis data, inhibition of TNF- α or IL-6 did not affect the expression of these genes (Figures S3C and S3D).

Taken together, these data suggest that SF can impact both the rate of glycolysis and the epigenomic landscape of CD4⁺ T cells, thereby contributing to the upregulation of disease-related H3K27ac-mediated chromatin remodeling independent of TNF- α or IL-6 signaling.

Glycolytic control of H3K27ac-mediated chromatin remodeling in JIA CD4⁺ T cells

To further evaluate the impact of glycolysis on H3K27ac changes during CD4⁺ T cell activation, we activated JIA SF CD4⁺ T cells for 24 h with or without 2-deoxy-D-glucose (2DG), an inhibitor

of glucose 6-phosphate production that thereby inhibits glycolysis. Employing ChIP-seq analysis targeting H3K27ac, we observed that inhibiting glycolysis prevented epigenome remodeling after CD4⁺ T cell activation (Figure 4A). Inhibition of glycolysis markedly decreased histone acetylation after T cell activation in JIA SF T cells (Figures 4B and 4C). Genes affected by inhibition of glycolysis in SF-derived JIA T cells were found to correlate with the genes upregulated during T cell activation in SF compared to PB healthy T cells (Figure 4D). Moreover, inhibition of glycolysis significantly affected genes associated with CD4⁺ T cell activation and function (Figure 4E). The majority of peaks affected by 2DG treatment in SF JIA T cells are annotated as promoter regions (Figure 4F). In contrast, HC T cells exhibit a distinct pattern, with only approximately 25% of the regions affected by glycolysis inhibition during activation being identified as promoter regions (Figure S4A). This observation was supported by an examination of transcription factor binding sites associated with these peaks (Figures 4G and S4B). Again, these results show that the impact of inhibiting glycolysis on promoter regions was more pronounced in SF JIA T cells compared to PB T cells (Figure S4C). These findings support a role of glycolysis in driving dysregulation of H3K27ac-associated promoter regions during activation in SF from patients with JIA.

Essential role of pyruvate-derived acetyl-CoA in mediating SF-driven changes in H3K27ac

To gain further insight into the role of glycolysis in the activation of disease-related acetylated regions, HC CD4⁺ T cells were activated for 24 h with anti-CD3/CD28 in the presence of either plasma or JIA SF with the addition of 2DG or oligomycin. Activation of CD4⁺ T cells in the presence of JIA SF resulted in a significant increase in H3K27ac levels at JIA SF-specific promoters compared to cells activated with plasma alone (Figure 5A). Importantly, this increase in H3K27ac was found to be dependent on glycolytic flux rather than oxidative phosphorylation (OXPHOS), as shown by the inhibition observed with 2DG but not oligomycin. To further validate these findings, gene expression was evaluated by RT-qPCR. Increased H3K27ac levels were indeed associated with elevated gene expression. Furthermore, the inhibition of glycolysis had a more pronounced impact on gene expression compared to the inhibition of OXPHOS (Figure 5B). To evaluate dose dependency, we measured the expression of *IL10RA*, *TRPS1*, *PNRC1*, *CD74*, and *CD80* in HC CD4⁺ T cells activated in the presence of SF with different concentrations of 2DG (50, 25, and 5 mM). The results demonstrated a dose-dependent inhibition of gene transcription, with lower concentrations of 2DG still significantly affecting gene expression (Figure S4d). To confirm that the inhibition of glycolysis specifically impacts the expression of JIA SF-induced genes, we measured the expression of *IL10RA*, *TRPS1*, *PNRC1*, *CD74*, and *CD80* in HC CD4⁺ T cells activated with SF in the presence of 3-(3-Pyridinyl)-1-(4-pyridinyl)-2-propen-1-one (3PO), an inhibitor of PFKFB3, a key glycolytic enzyme. Our

(G) Selected genes upregulated in activated JIA SF-derived CD4⁺ T cells.

(H) RT-qPCR measured mRNA expression of *IL10RA*, *TRPS1*, *PNRC1*, *CD74*, and *CD80* in human CD4⁺ T cells from HC PB or JIA SF cells activated for 24 h with anti-CD3/CD28.

All graphs represent mean \pm SD. One-way ANOVA or Student's t test measured statistical significance. * p < 0.05, ** p < 0.01, *** p < 0.001, **** p < 0.0001.

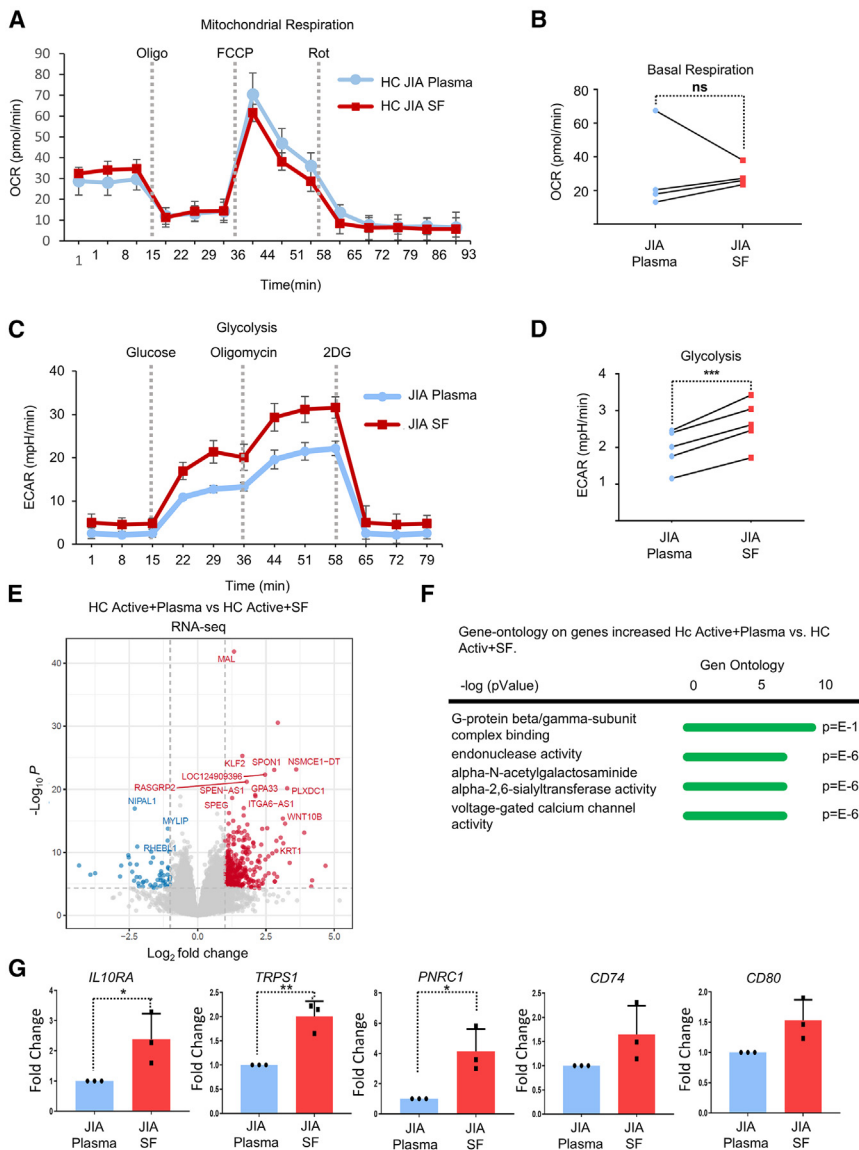


Figure 3. JIA SF promotes metabolic re-programming and H3K27ac landscape re-modeling

(A and B) HC PB CD4⁺ T cells were activated for 20 h with anti-CD3/CD28 in the presence of JIA SF or plasma (30%), and OCRs were measured by Seahorse technology.

(C and D) HC PB CD4⁺ T cells were activated for 20 h with anti-CD3/CD28 in the presence of JIA SF or plasma (30%), and ECARs were measured by Seahorse technology.

(E) Volcano plot showing differentially expressed genes between activated (anti-CD3/CD28, 24 h) HC PB CD4⁺ T cells in the presence of JIA SF or plasma (30%), where red dots indicate genes with an FDR of less than 0.05.

(F) Enriched GO terms for the upregulated genes in activated CD4⁺ T cells in the presence of SF.

(G) ChIP-qPCR of *IL10R*, *TRPS1*, *PNRC1*, *CD74*, and *CD80* promotor regions from human healthy CD4⁺ T cells activated with anti-CD3/CD28 in the presence of JIA SF or plasma (30%).

All graphs represent mean \pm SD. Student's t test measured statistical significance. *p < 0.05, **p < 0.01.

and SB204990 did not affect *IL10RA*, *TRPS1*, *PNRC1*, or *CD74* expression, only affecting the expression of *CD80* (Figure S5B).

This observation, along with the lack of effect from ATP synthase and ACLY inhibition, strongly suggests that extra-mitochondrial pyruvate metabolism is a key driver of histone acetylation during CD4⁺ T cell activation in the pro-inflammatory SF environment.

DISCUSSION

Autoimmune diseases are associated with aberrant autoreactive immune cells that lead to tissue damage, resulting in increased morbidity and mortality. The intracellular metabolism of immune cell populations undergoes significant alterations in the context of autoimmunity, and concurrently, the epigenome often exhibits distinct remodeling.^{3,4,21–23} While these individual phenomena are well documented, the molecular mechanisms connecting immune cell metabolism with specific changes in the epigenetic landscape remain unclear.

Considerable evidence supports a critical role of glycolysis during T cell activation, differentiation, and function.^{24–30} In the context of autoimmune disease, inhibition of glycolysis has shown promising effects, specifically in the context of RA. Studies indicate that suppressing glycolysis can reduce disease severity in autoimmune disease mouse model models.^{31–34} However, there is an absence of mechanistic studies evaluating the direct connection between altered intracellular metabolism and epigenetic reprogramming in pathogenic T cells isolated

results showed that 3PO inhibited gene transcription similarly as 2DG, further supporting a crucial role of glycolysis in regulating the expression of these JIA SF-related genes (Figure 5C).

Previously, we established a crucial role for extra-mitochondrial pyruvate metabolism in CD4⁺ T cell activation-induced epigenome remodeling.⁶ To evaluate this further, PB CD4⁺ T cells obtained from healthy donors were activated by anti-CD3/CD28 stimulation for 24 h in the presence of SF with or without pharmacological inhibition of pyruvate dehydrogenase 6,8-bis(benzylthio) octanoic acid. Inhibition of PDH activity resulted in a significant decrease in the expression of JIA-related genes in a dose-dependent manner (Figures 5C and S5A).

To evaluate whether the observed effects on gene expression induced by SF were specifically related to PDH and not other enzymes involved in acetyl-CoA production, such as ATP-citrate lyase (ACLY), we activated CD4⁺ T cells in the presence of JIA SF and the ACLY inhibitor BMS303141 or SB204990. BMS303141

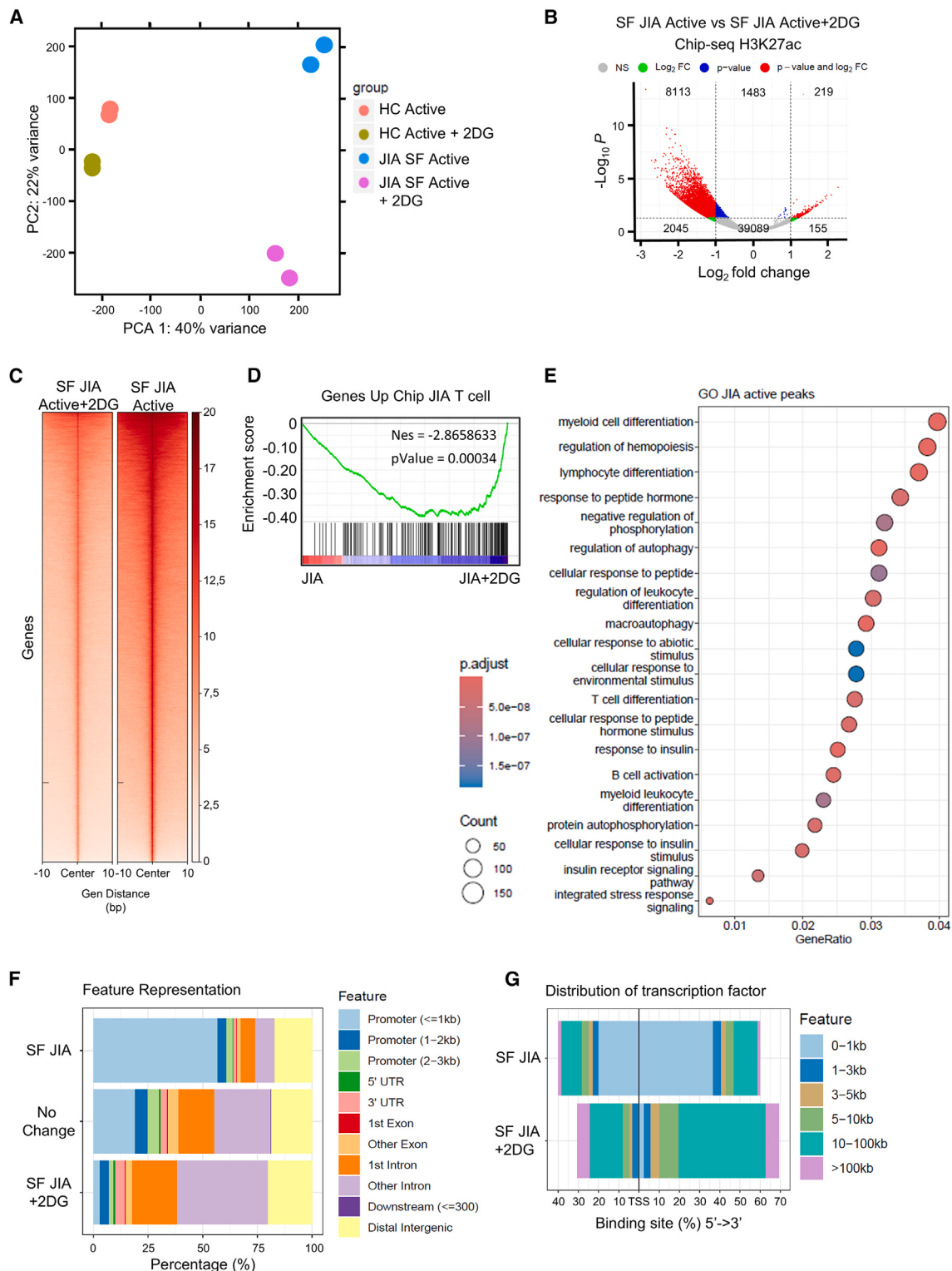


Figure 4. Glycolytic modulation of H3K27ac-driven chromatin remodeling in JIA CD4⁺ T cells

(A) Principal-component analysis based on H3K27ac signal.

(B) Volcano plots of H3K27ac signal, based on comparisons of all replicates within the depicted groups. Red dots indicate open regions with an FDR < 0.05.

(C) Plot of the percentages of significantly decreased H3K27ac peaks on the JIA T cells activated in the presence of 2DG.

(legend continued on next page)

directly from inflammatory environments. Additionally, for JIA, there have been no studies that have explored the metabolic profile of SF CD4⁺ T cells. Here, we demonstrate that inhibition of glycolysis during the activation of SF-derived CD4⁺ T cells is effective in preventing H3K27ac landscape remodeling (Figures 4A–4D). Notably, this effect is particularly pronounced in H3K27ac-associated promoter regions (Figures 4E and 4F). Furthermore, the effect of inhibiting glycolysis is more robust on the promoter regions of JIA SF T cells compared to HC T cells (Figures S4A and S4B).

Increased glucose uptake plays a pivotal role in various aspects of T cell biology, including development, proliferation, and function, as demonstrated in several studies.^{17,24,30,35–37} Notably, T cells deficient in Glut1 glucose transport exhibit impaired proliferation.²⁴ In this context, our data demonstrate that JIA SF CD4⁺ T cells exhibit heightened glycolytic activity and increased acetyl-CoA production compared to T cells from the PB of the same individual or HCs (Figures 1D–1F). This finding contrasts with the metabolic behavior of PB CD4⁺ T cells in patients with RA, which undergo a fundamental shift in glucose utilization, favoring diversion away from pyruvate and lactate production and toward the pentose phosphate pathway.^{12,33,38} Furthermore, RA T cells have been reported to be unable to maintain the NAD⁺ coenzyme pool in the mitochondria, which subsequently affects the TCA cycle and aspartate production.¹¹ Our findings reveal a distinctive metabolic signature in T cells isolated from the SF of patients with JIA. Notably, we observed no significant defects in the production of malate and fumarate metabolites within the TCA cycle when comparing JIA SF and HC T cells (Figure 1A). Our Seahorse experiments also indicate no substantial differences in mitochondrial respiration between JIA SF or PB T cells and HC PB T cells (Figures 1B and 1C). These observations demonstrate distinct metabolic signatures that vary between disease and CD4⁺ T cell location.

In the context of JIA, recent evidence has revealed that SF has the capacity to induce polarization toward Th1 cells, characterized as proinflammatory T helper cells.² Here, we demonstrate that the exposure of HC T cells to SF induces a significant increase in glycolytic activity compared to controls (Figures 3C and 3D). This increase in glycolytic response is not mirrored by an increase in mitochondrial respiration (Figures 3A and 3B), showing a selective influence of SF on the glycolytic pathway. The complexity of SF means that pinpointing a singular component responsible for induction of glycolysis in these cells is challenging. Although SF is known to contain elevated levels of TNF- α and IL-6,²⁰ our data indicate that the glycolytic response triggered by SF is independent of these cytokines (Figure S3A and S3D). However, glycolysis-mediated alterations in the H3K27ac landscape likely play a role in the development of pro-inflammatory SF T helper cells.

Previously, we undertook a comprehensive exploration of enhancer and super-enhancer signatures using H3K27ac chromatin immunoprecipitation in CD4⁺ T cells derived from the SF of patients with JIA.³ These findings demonstrated that acetyla-

tedregion profiles can vary significantly between subsets of T cells, particularly T_{mem}/T_{eff} cells, isolated from HCs and those from patients with JIA. Our current study reveals that this altered H3K27ac landscape persists even after *ex vivo* T cell activation. We observed significant enrichment of ETS family transcription factors at JIA-associated promoters, which may reflect an exaggerated activation or pro-inflammatory state in these cells. Given that ETS factors are commonly involved in driving inflammatory gene expression, their high prevalence in SF JIA T cells suggests a transcriptional environment primed for sustained inflammation (Figure 2F).^{39–46} In contrast, HC T cells showed enrichment of transcription factors from a diverse array of families (bHLH, AP2/EREBP, MYB-related, and Zf), indicating a broader range of regulatory mechanisms that may help maintain a balanced immune response in healthy individuals (Figure S1F). The reduced diversity of transcription factor families in JIA T cells could contribute to their dysregulated activation, limiting their ability to appropriately modulate or resolve inflammatory responses.

In our previous work, we were unable to determine whether aberrant acetylated region profiles are causally related to JIA disease pathogenesis or merely the consequence of the local proinflammatory environment. Here, we evaluated the direct influence of the environment on the transcriptome and on the epigenetic landscape. Our findings reveal that SF exposure was sufficient to alter the gene expression and H3K27ac landscape of HC T cells, upregulating gene expression linked to immune responses. Additionally, in activated cells, it amplifies the expression of genes involved in T cell activation pathways, particularly those associated with G-protein signaling and calcium channels, which play key roles in metabolic regulation (Figures 3E, 3F, S2E, and S2F).⁴⁷ Notably, this exposure leads to the acetylation of regions identified previously as active in JIA SF T cells (Figure 3G). As mentioned previously, we show an enrichment of JIA-associated promoters for ETS family binding motifs. The ETS family can be activated by proinflammatory signals, such as TNF- α , IL-1, and transforming growth factor β , cytokines present in the SF.^{48–50} In this way, the pro-inflammatory SF environment can promote chromatin remodeling through glycolysis-driven changes in H3K27ac, priming acetylated regions for subsequent cytokine-mediated transcription factor activation.

Recently, we identified nuclear pyruvate dehydrogenase (PDH) as an important metabolic complex that facilitates histone acetylation and transcriptional activation after TCR engagement.⁶ The generation of pyruvate and the translocation of PDH to the nucleus was identified as a pivotal step indispensable for producing acetyl-CoA, which, in turn, is essential for the remodeling of acetylated regions triggered by T cell activation. PDH has also been found to be essential for histone acetylation and subset-specific gene expression in Th17 cells.⁵ In this study, we demonstrate that PDH inhibition and not ACLY abrogates the expression of SF-induced genes (Figures 5B, S5A, and S5B). These findings not only emphasize the importance of PDH in this context but also support potential therapeutic interventions involving PDH.

(D) GSEA comparing the H3K27ac signal in the T cell gene set of JIA CD4⁺ T cells to the ChIP-seq data of JIA T CD4⁺ cells treated with 2DG.

(E) GO terms are ranked by enrichment scores of genes (Es) that are upregulated in JIA-activated CD4⁺ T cells versus those activated in the presence of 2DG.

(F) Genomic distribution of peaks identified in ChIP-seq data.

(G) Distribution of TF-binding loci relative to 5' ends of genes.

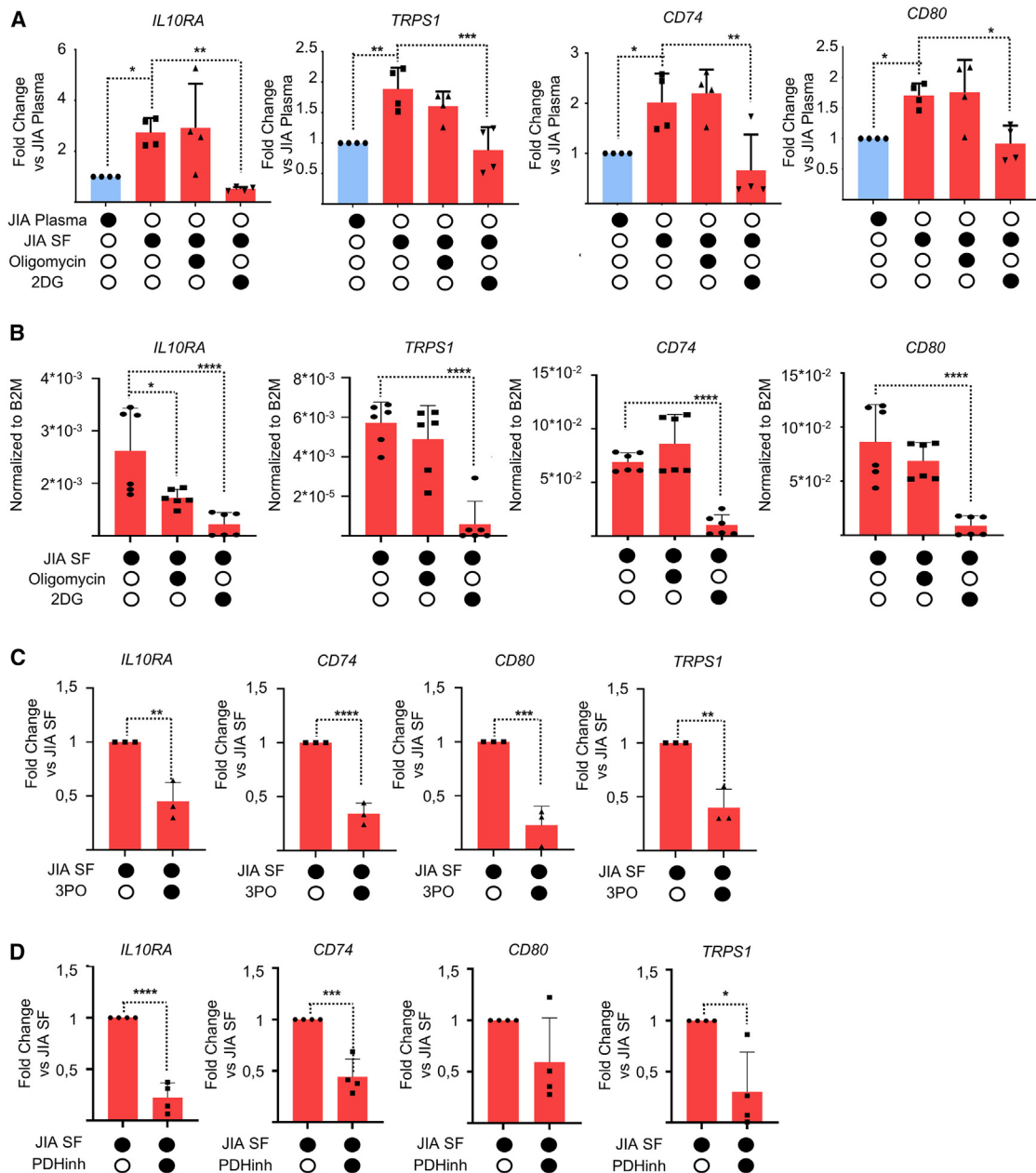


Figure 5. Glycolysis-driven pyruvate metabolism is required for SF-mediated changes in H3K27ac

(A) ChIP-qPCR of *IL10R*, *TRPS1*, *PNRC1*, *CD74*, and *CD80* promotor regions from human CD4⁺ T cells activated with anti-CD3/CD28 in the presence of JIA SF or plasma (30%) and in the presence or absence of oligomycin or 2DG for 20 h.

(B) mRNA expression of *IL10RA*, *TRPS1*, *PNRC1*, *CD74*, and *CD80* was measured by RT-qPCR in human CD4⁺ T cells from HC PB in the presence of JIA SF, oligomycin or 2DG cells activated for 24 h with anti-CD3/CD28.

(C) mRNA expression of *IL10RA*, *TRPS1*, *CD74*, and *CD80* was measured by RT-qPCR in human CD4⁺ T cells from HC PB in the presence of JIA SF and 3-(3-pyridinyl)-1-(4-pyridinyl)-2-propen-1-one (3PO) cells activated for 24 h with anti-CD3/CD28.

(D) mRNA expression of *IL10RA*, *TRPS1*, *CD74*, and *CD80* was measured by RT-qPCR in human CD4⁺ T cells from HC PB in the presence of JIA SF and 6,8-bis(benzylthio) octanoic acid (a PDH inhibitor) cells activated for 24 h with anti-CD3/CD28.

All graphs represent mean ± SD. One-way ANOVA or Student's t test measured statistical significance. *p < 0.05, **p < 0.01, ***p < 0.001, ****p < 0.0001.

inhibition for the benefit of patients with JIA. Inhibition of PDH has been explored in the context of conditions such as acute myeloid leukemia, where it leads to decreased glycolysis and increased

reliance on oxidative phosphorylation.⁵¹ However, the potential application of PDH inhibitors within the autoimmune disease context remains unexplored. We propose that this approach

may offer reduced toxicity and increased specificity compared to the use of glycolysis inhibitors.

Taken together, our observations suggest that the pro-inflammatory synovial environment results in metabolic dysfunction which can disrupt the epigenetic landscape, resulting in transcriptional reprogramming. The dependence of activated T cells on pyruvate production through glycolysis to modulate the H3K27ac landscape and promoter activity further supports targeting T cell glycolysis to suppress inflammatory responses and promote tolerance and immune suppression.

Limitations of the study

Our study has several limitations that should be mentioned. First, we did not directly measure T cell metabolism and the epigenome immediately after isolation from SF. To minimize environmental influence, T cells isolated from patient joints were rested for 24 h and then activated with CD3/CD28 *in vitro*. However, analyzing metabolic and epigenetic profiles directly post isolation and compared with the data from our study would offer a clearer representation of the T cell state in the synovial environment, and future studies could aim to include these direct assessments.

Second, while we evaluated glycolysis in T cells activated in the presence of SF using the Seahorse assay, which measures extracellular acidification as a proxy for lactate production, this approach provides an indirect estimate of glycolytic flux. To obtain a more precise profile of lactate levels and a broader understanding of metabolic byproducts, techniques such as MS would be beneficial. This approach could yield a more detailed picture of the effects of JIA SF on the metabolism of healthy PB T cells.

Last, all T cell experiments in this study used polyclonal activation via CD3/CD28, which may not fully capture the complexity of *in vivo* immune activation. Co-culturing T cells with dendritic cells in the presence of SF may better mimic physiological conditions and provide additional information concerning the impact of SF on both cell types' metabolism and epigenome. Future studies incorporating dendritic cell-T cell co-cultures in the presence of SF could thus provide valuable insights into the cell-specific and interactive metabolic responses within the inflamed joint environment.

RESOURCE AVAILABILITY

Lead contact

Requests for further information, resources, and reagents should be directed to and will be fulfilled by the lead contact, Paul Coffer (pcoffer@umcutrecht.nl).

Materials availability

This study did not generate new unique reagents.

Data and code availability

- The RNA-seq and ChIP-seq data have been deposited at EGA: EGAS50000000808 and are publicly available as of the date of publication. Accession numbers are listed in the [key resources table](#).
- All other data reported in this paper will be shared by the [lead contact](#) upon request.
- This paper does not report original code.
- Any additional information required to reanalyze the data reported in this paper is available from the [lead contact](#) upon request.

ACKNOWLEDGMENTS

We are grateful to all the authors of this paper for their contributions and significant efforts in completing and publishing this research. We would like to extend special thanks to Bas Vastert and Jorg van Loosdregt for giving us access to patient samples and for the scientific discussions, Can Gulersonmez and Edwin Stigter from the metabolomics facility of UMC for scientific discussions and for their assistance with the metabolomics studies performed in this study, and Theo Chalkiadakis and Stefan Prekovic for their invaluable assistance with the RNA-seq and ChIP-seq analyses performed in this study. Finally, we would like to thank all members of the Coffer Lab for their valuable discussions concerning this work. This work is supported by grants from the Stichting WKZ Foundation (2016) and ReumaNederland (11-19-18 and 18-01-401).

AUTHOR CONTRIBUTIONS

The experiments were mainly performed by E.M. with the assistance of E.C. Part of the Seahorse experiments with SF was performed by B.V. The metabolomics studies were conducted by E.S. and C.G. T.C. and S.P. analyzed the RNA-seq and ChIP-seq data. SF extraction from patient samples was carried out by B.V. The scientific discussions led by J.v.L. and B.V. were highly valuable in generating hypotheses and improving the overall experimental design. The study was designed and written by E.M. and P.J.C.

DECLARATION OF INTERESTS

The authors declare no competing interests.

STAR METHODS

Detailed methods are provided in the online version of this paper and include the following:

- [KEY RESOURCES TABLE](#)
- [EXPERIMENTAL MODEL AND STUDY PARTICIPANT DETAILS](#)
 - Patient details
 - Collection of healthy control peripheral blood samples
- [METHOD DETAILS](#)
 - Cell isolation and culture
 - Chromatin-immunoprecipitation (ChIP)
 - DNA-RNA-sequencing
 - ChIP-qPCR
 - Real-Time PCR
 - Seahorse assays
 - Measurements of acetyl-CoA levels
 - Sample preparation and LC-MS measurement of glycolytic/TCA cycle intermediates
- [QUANTIFICATION AND STATISTICAL ANALYSIS](#)
 - Statistical analysis

SUPPLEMENTAL INFORMATION

Supplemental information can be found online at <https://doi.org/10.1016/j.celrep.2025.115287>.

Received: February 27, 2024

Revised: November 11, 2024

Accepted: January 17, 2025

Published: February 18, 2025

REFERENCES

1. Prakken, B., Albani, S., and Martini, A. (2011). Juvenile idiopathic arthritis. *Lancet* 377, 2138–2149.
2. Julé, A.M., Hoyt, K.J., Wei, K., Gutierrez-Arcelus, M., Taylor, M.L., Ng, J., Lederer, J.A., Case, S.M., Chang, M.H., Cohen, E.M., and Dedeoglu, F.

- (2021). Th1 polarization defines the synovial fluid T cell compartment in oligoarticular juvenile idiopathic arthritis. *JCI Insight* 6.
3. Peeters, J.G.C., Vervoort, S.J., Tan, S.C., Mijnheer, G., de Roock, S., Vastert, S.J., Nieuwenhuis, E.E.S., van Wijk, F., Prakken, B.J., Creyghton, M.P., et al. (2015). Inhibition of Super-Enhancer Activity in Autoinflammatory Site-Derived T Cells Reduces Disease-Associated Gene Expression. *Cell Rep.* 12, 1986–1996.
 4. Shyer, J.A., Flavell, R.A., and Bailis, W. (2020). Metabolic signaling in T cells. *Cell Res.* 30, 649–659.
 5. Soriano-Baguet, L., Grusdat, M., Kurniawan, H., Benzarti, M., Binsfeld, C., Ewen, A., Longworth, J., Bonetti, L., Guerra, L., Franchina, D.G., et al. (2023). Pyruvate dehydrogenase fuels a critical citrate pool that is essential for Th17 cell effector functions. *Cell Rep.* 42, 112153.
 6. Mocholi, E., Russo, L., Gopal, K., Ramstead, A.G., Hochrein, S.M., Vos, H.R., Geeven, G., Adegoke, A.O., Hoekstra, A., van Es, R.M., et al. (2023). Pyruvate metabolism controls chromatin remodeling during CD4+ T cell activation. *Cell Rep.* 42, 112583.
 7. Chang, C.-H., Curtis, J.D., Maggi, L.B., Jr., Faubert, B., Villarino, A.V., O'Sullivan, D., Huang, S.C.C., van der Windt, G.J.W., Blagih, J., Qiu, J., et al. (2013). Posttranscriptional control of T cell effector function by aerobic glycolysis. *Cell* 153, 1239–1251.
 8. Peng, M., Yin, N., Chhangawala, S., Xu, K., Leslie, C.S., and Li, M.O. (2016). Aerobic glycolysis promotes T helper 1 cell differentiation through an epigenetic mechanism. *Science* 354, 481–484.
 9. Weyand, C.M., Wu, B., and Goronzy, J.J. (2020). The metabolic signature of T cells in rheumatoid arthritis. *Curr. Opin. Rheumatol.* 32, 159–167.
 10. Weyand, C.M., and Goronzy, J.J. (2020). Immunometabolism in the development of rheumatoid arthritis. *Immunol. Rev.* 294, 177–187.
 11. Wu, B., Zhao, T.V., Jin, K., Hu, Z., Abdel, M.P., Warrington, K.J., Goronzy, J.J., and Weyand, C.M. (2021). Mitochondrial aspartate regulates TNF biogenesis and autoimmune tissue inflammation. *Nat. Immunol.* 22, 1551–1562.
 12. Yang, Z., Fujii, H., Mohan, S.V., Goronzy, J.J., and Weyand, C.M. (2013). Phosphofructokinase deficiency impairs ATP generation, autophagy, and redox balance in rheumatoid arthritis T cells. *J. Exp. Med.* 210, 2119–2134.
 13. Shen, Y., Wen, Z., Li, Y., Matteson, E.L., Hong, J., Goronzy, J.J., and Weyand, C.M. (2017). Metabolic control of the scaffold protein TKS5 in tissue-invasive, proinflammatory T cells. *Nat. Immunol.* 18, 1025–1034.
 14. Li, Y., Shen, Y., Jin, K., Wen, Z., Cao, W., Wu, B., Wen, R., Tian, L., Berry, G.J., Goronzy, J.J., and Weyand, C.M. (2019). The DNA Repair Nuclease MRE11A Functions as a Mitochondrial Protector and Prevents T Cell Pyroptosis and Tissue Inflammation. *Cell Metabol.* 30, 477–492.e6.
 15. Shervington, L., Darekar, A., Shaikh, M., Mathews, R., and Shervington, A. (2018). Identifying Reliable Diagnostic/Predictive Biomarkers for Rheumatoid Arthritis. *Biomark. Insights* 13, 1177271918801005.
 16. Kim, T.-H., Choi, S.J., Lee, Y.H., Song, G.G., and Ji, J.D. (2012). Combined therapeutic application of mTOR inhibitor and vitamin D(3) for inflammatory bone destruction of rheumatoid arthritis. *Med. Hypotheses* 79, 757–760.
 17. Laragione, T., and Gulko, P.S. (2010). mTOR regulates the invasive properties of synovial fibroblasts in rheumatoid arthritis. *Mol. Med.* 16, 352–358.
 18. Clunton, A.A., Huang, H., Dai, L., Liu, X., Zhao, Y., and Locasale, J.W. (2015). The rate of glycolysis quantitatively mediates specific histone acetylation sites. *Cancer Metabol.* 3, 10.
 19. Creyghton, M.P., Cheng, A.W., Welstead, G.G., Kooistra, T., Carey, B.W., Steine, E.J., Hanna, J., Lodato, M.A., Frampton, G.M., Sharp, P.A., et al. (2010). Histone H3K27ac separates active from poised enhancers and predicts developmental state. *Proc. Natl. Acad. Sci. USA* 107, 21931–21936.
 20. de Jager, W., Hoppenreijns, E.P.A.H., Wulffraat, N.M., Wedderburn, L.R., Kuis, W., and Prakken, B.J. (2007). Blood and synovial fluid cytokine signatures in patients with juvenile idiopathic arthritis: a cross-sectional study. *Ann. Rheum. Dis.* 66, 589–598.
 21. Wu, B., Goronzy, J.J., and Weyand, C.M. (2020). Metabolic Fitness of T Cells in Autoimmune Disease. *Immunometabolism* 2, e200017.
 22. MacLver, N.J., Michalek, R.D., and Rathmell, J.C. (2013). Metabolic Regulation of T Lymphocytes. *Annu. Rev. Immunol.* 31, 259–283.
 23. Chi, H. (2022). Immunometabolism at the intersection of metabolic signaling, cell fate, and systems immunology. *Cell. Mol. Immunol.* 19, 299–302.
 24. Macintyre, A.N., Gerriets, V.A., Nichols, A.G., Michalek, R.D., Rudolph, M.C., Deoliveira, D., Anderson, S.M., Abel, E.D., Chen, B.J., Hale, L.P., and Rathmell, J.C. (2014). The glucose transporter Glut1 is selectively essential for CD4 T cell activation and effector function. *Cell Metabol.* 20, 61–72.
 25. Lunt, S.Y., and Vander Heiden, M.G. (2011). Aerobic glycolysis: meeting the metabolic requirements of cell proliferation. *Annu. Rev. Cell Dev. Biol.* 27, 441–464.
 26. Wang, Y., Tao, A., Vaeth, M., and Feske, S. (2020). Calcium regulation of T cell metabolism. *Curr. Opin. Physiol.* 17, 207–223.
 27. O'Neill, L.A.J., Kishton, R.J., and Rathmell, J. (2016). A guide to immunometabolism for immunologists. *Nat. Rev. Immunol.* 16, 553–565.
 28. Bauer, D.E., Harris, M.H., Plas, D.R., Lum, J.J., Hammerman, P.S., Rathmell, J.C., Riley, J.L., and Thompson, C.B. (2004). Cytokine stimulation of aerobic glycolysis in hematopoietic cells exceeds proliferative demand. *Faseb. J.* 18, 1303–1305.
 29. Hochrein, S.M., Wu, H., Eckstein, M., Arrigoni, L., Herman, J.S., Schumacher, F., Gerecke, C., Rosenfeldt, M., Grün, D., Kleuser, B., et al. (2022). The glucose transporter GLUT3 controls T helper 17 cell responses through glycolytic epigenetic reprogramming. *Cell Metabol.* 34, 516–532.e11.
 30. Wang, R., Dillon, C.P., Shi, L.Z., Milasta, S., Carter, R., Finkelstein, D., McCormick, L.L., Fitzgerald, P., Chi, H., Munger, J., and Green, D.R. (2011). The transcription factor Myc controls metabolic reprogramming upon T lymphocyte activation. *Immunity* 35, 871–882.
 31. Choi, S.-C., Titov, A.A., Abboud, G., Seay, H.R., Brusko, T.M., Roopenian, D.C., Salek-Ardakani, S., and Morel, L. (2018). Inhibition of glucose metabolism selectively targets autoreactive follicular helper T cells. *Nat. Commun.* 9, 4369.
 32. Mangal, J.L., Inamdar, S., Le, T., Shi, X., Curtis, M., Gu, H., and Acharya, A.P. (2021). Inhibition of glycolysis in the presence of antigen generates suppressive antigen-specific responses and restrains rheumatoid arthritis in mice. *Biomaterials* 277, 121079.
 33. Abboud, G., Choi, S.C., Kanda, N., Zeumer-Spataro, L., Roopenian, D.C., and Morel, L. (2018). Inhibition of Glycolysis Reduces Disease Severity in an Autoimmune Model of Rheumatoid Arthritis. *Front. Immunol.* 9, 1973.
 34. Yin, Y., Choi, S.C., Xu, Z., Zeumer, L., Kanda, N., Croker, B.P., and Morel, L. (2016). Glucose Oxidation Is Critical for CD4+ T Cell Activation in a Mouse Model of Systemic Lupus Erythematosus. *J. Immunol.* 196, 80–90.
 35. Shi, L.Z., Wang, R., Huang, G., Vogel, P., Neale, G., Green, D.R., and Chi, H. (2011). HIF1alpha-dependent glycolytic pathway orchestrates a metabolic checkpoint for the differentiation of TH17 and Treg cells. *J. Exp. Med.* 208, 1367–1376.
 36. Blagih, J., Coulombe, F., Vincent, E.E., Dupuy, F., Galicia-Vázquez, G., Yurchenko, E., Raissi, T.C., van der Windt, G.J.W., Viollet, B., Pearce, E.L., et al. (2015). The energy sensor AMPK regulates T cell metabolic adaptation and effector responses in vivo. *Immunity* 42, 41–54.
 37. Ho, P.-C., Bihuniak, J.D., Macintyre, A.N., Staron, M., Liu, X., Amezquita, R., Tsui, Y.C., Cui, G., Micevic, G., Perales, J.C., et al. (2015). Phosphoenolpyruvate Is a Metabolic Checkpoint of Anti-tumor T Cell Responses. *Cell* 162, 1217–1228.
 38. Tsokos, G.C. (2016). Metabolic control of arthritis: Switch pathways to treat. *Sci. Transl. Med.* 8, 331fs8.
 39. Garrett-Sinha, L.A., Kearly, A., and Satterthwaite, A.B. (2016). The Role of the Transcription Factor Ets1 in Lupus and Other Autoimmune Diseases. *Crit. Rev. Immunol.* 36, 485–510.

40. Malin, J., Martinez-Ruiz, G.U., Zhao, Y., Shissler, S.C., Cowan, J.E., Ding, Y., Morales-Sánchez, A., Ishikawa, M., Lavaert, M., Das, A., et al. (2023). Expression of the transcription factor Klf6 by thymic epithelial cells is required for thymus development. *Sci. Adv.* 9, eadg8126.
41. Palau, N., Julià, A., Ferrández, C., Puig, L., Fonseca, E., Fernández, E., López-Lasanta, M., Tortosa, R., and Marsal, S. (2013). Genome-wide transcriptional analysis of T cell activation reveals differential gene expression associated with psoriasis. *BMC Genom.* 14, 825.
42. Korinskaya, S., Parameswaran, S., Weirauch, M.T., and Barski, A. (2021). Runx Transcription Factors in T Cells—What Is Beyond Thymic Development? *Front. Immunol.* 12, 701924.
43. Wong, W.F., Kohu, K., Nakamura, A., Ebina, M., Kikuchi, T., Tazawa, R., Tanaka, K., Kon, S., Funaki, T., Sugahara-Tobinai, A., et al. (2012). Runx1 deficiency in CD4+ T cells causes fatal autoimmune inflammatory lung disease due to spontaneous hyperactivation of cells. *J. Immunol.* 188, 5408–5420.
44. Trop-Steinberg, S., and Azar, Y. (2017). AP-1 Expression and its Clinical Relevance in Immune Disorders and Cancer. *Am. J. Med. Sci.* 353, 474–483.
45. Renoux, F., Stellato, M., Haftmann, C., Vogetseder, A., Huang, R., Subramanian, A., Becker, M.O., Blyszzuk, P., Becher, B., Distler, J.H.W., et al. (2020). The AP1 Transcription Factor Fosl2 Promotes Systemic Autoimmunity and Inflammation by Repressing Treg Development. *Cell Rep.* 31, 107826.
46. Hisanaga-Oishi, Y., Nishiwaki-Ueda, Y., Nojima, K., and Ueda, H. (2014). Analysis of the expression of candidate genes for type 1 diabetes susceptibility in T cells. *Endocr. J.* 61, 577–588.
47. Gudermann, T., and Bader, M. (2015). Receptors, G proteins, and integration of calcium signalling. *J. Mol. Med.* 93, 937–940.
48. de Jager, W., Prakken, B.J., Bijlsma, J.W.J., Kuis, W., and Rijkers, G.T. (2005). Improved multiplex immunoassay performance in human plasma and synovial fluid following removal of interfering heterophilic antibodies. *J. Immunol. Methods* 300, 124–135.
49. Redlich, K., Kiener, H.P., Schett, G., Tohidast-Akrad, M., Selzer, E., Radda, I., Stummvoll, G.H., Steiner, C.W., Gröger, M., Bitzan, P., et al. (2001). Over-expression of transcription factor Ets-1 in rheumatoid arthritis synovial membrane: regulation of expression and activation by interleukin-1 and tumor necrosis factor alpha. *Arthritis Rheum.* 44, 266–274.
50. Klunker, S., Chong, M.M.W., Mantel, P.Y., Palomares, O., Bassin, C., Ziegler, M., Rückert, B., Meiler, F., Akdis, M., Littman, D.R., and Akdis, C.A. (2009). Transcription factors RUNX1 and RUNX3 in the induction and suppressive function of Foxp3+ inducible regulatory T cells. *J. Exp. Med.* 206, 2701–2715.
51. Anderson, R., Pladna, K.M., Schramm, N.J., Wheeler, F.B., Kridel, S., and Pardee, T.S. (2023). Pyruvate Dehydrogenase Inhibition Leads to Decreased Glycolysis, Increased Reliance on Gluconeogenesis and Alternative Sources of Acetyl-CoA in Acute Myeloid Leukemia. *Cancers* 15, 484.
52. Petty, R.E., Southwood, T.R., Manners, P., Baum, J., Glass, D.N., Goldenberg, J., He, X., Maldonado-Cocco, J., Orozco-Alcalá, J., Prieur, A.M., et al. (2004). International League of Associations for Rheumatology classification of juvenile idiopathic arthritis: second revision, Edmonton, 2001. *J. Rheumatol.* 31, 390–392.
53. Petty, R.E., Southwood, T.R., Baum, J., Bhettay, E., Glass, D.N., Manners, P., Maldonado-Cocco, J., Suarez-Almazor, M., Orozco-Alcalá, J., and Prieur, A.M. (1998). Revision of the proposed classification criteria for juvenile idiopathic arthritis: Durban, 1997. *J. Rheumatol.* 25, 1991–1994.

STAR★METHODS

KEY RESOURCES TABLE

REAGENT or RESOURCE	SOURCE	IDENTIFIER
Antibodies		
Anti-Human-CD3	eBioscience	Cat# 16-0037; RRID: AB_468854
Anti-human CD28	eBioscience	Cat# 16-0289-85; RRID: AB_468926
Anti-Mouse CD28 Functional	eBioscience	Cat# 16-0281-85; RRID: AB_468921
Anti-mouse CD3	eBioscience	Cat# 16-0031-85; RRID: AB_468847
Anti-Histone H3-acetyl K27	Abcam	Cat# ab4729
Chemicals, peptides, and recombinant proteins		
PBS (1X) without Ca++, Mg++, 500mL	Lonza	# BE17-516F
FBS	Biowest	Cat# S1810-500 Lot# S14068S1810
Penicillin-Streptomycin	Gibco	# 15-140-122
L-Glutamine	Lonza	# BE17-605E
2-Mercaptoethanol	Gibco	# 11508916
Methanol	Sigma-Aldrich	# 1060351000
Hyaluronidase	Sigma-Aldrich	#H4272-30MG
RPMI + glutamax	Gibco	# 61870044
RPMI 1640 Medium, no glucose	Gibco	# 11879020
2-Deoxy-D-glucose	Sigma-Aldrich	#D8375-5G
oligomycin	Merck Millipore	# 495455
FCCP, mitochondrial oxidative phosphorylation uncoupler	Abcam	# ab120081
Rotenone	Merck Millipore	#R8875
3PO ≥ 98% (HPLC)	Sigma-Aldrich	# SML1343
6,8-Bis(benzylthio)-octanoic acid	Sigma-Aldrich	# SML0404
Sodium Pyruvate	Thermo Fisher	# 11360070
SB204990	Med Chem Express	# HY-16450
BMS303141	Sigma-Aldrich	# SML0784
HEPES	Sigma-Aldrich	#H4034-100G
Bovine serum albumin (BSA)	Sigma-Aldrich	#A9647-500G
D-(+)-Glucose solution	Sigma-Aldrich	#G8769-100ML
DMSO	Sigma-Aldrich	#D2650
Ficoll® Paque Plus	Sigma-Aldrich	# GE17-1440-02
SYBR	Thermo fisher	#S33102
iScript cDNA kit	biorad	#170-8891
Formaldehyde	Sigma-Aldrich	#252549-1L
D-(+)-Glucose solution	Sigma-Aldrich	#G8769-100ML
Tween 20	Sigma-Aldrich	#P7949-500ML
HALT protease inhibitor	Thermo scientific	#78439
Powdered milk	Carl Roth	#T145.2
Pierce™ Protein A/G Magnetic Beads	Thermo fisher	#88802
Proteinase K, recombinant, PCR Grade	Sigma	#3115828001
RNeasy Mini Kit	Qiagen	#74106
Seahorse XF DMEM medium	Agilent Technologies	#103575-100
Adalimumab (anti-TNF-alpha)	Selleckchem	# A2010
Etanercept (TNF-Inhibitor)	MCE	# HY-108847

(Continued on next page)

Continued

REAGENT or RESOURCE	SOURCE	IDENTIFIER
Tocilizumab (anti-IL-6R)	Selleckchem	# A2012
Critical commercial assays		
MagniSort™ Human CD4 ⁺ T cell Enrichment Kit	eBioscience	#8804-6811-74
CD4 (L3T4) MicroBeads, mouse	Miltenyi	# 130-117-043
T cell TransAct, Human	Miltenyi	#130-111-160
seahorse XFe24 Flux Packs	Agilent	#1023-40-100
Acetyl-CoA Assay Kit	Biovision, Milpitas CA	#K317-100
chip DNA clean & concentrator	zymo research	#D5205
IL2 elisa	Biolegend	#431804
EAE induction kit: MOG35-55/CFA Emulsion PTX	Hooke Laboratories, Inc	#EK-2110
Deposited data		
RNA-seq	EGA	ID: EGAS50000000808
Chip-seq	EGA	ID: EGAS50000000808
Oligonucleotides		
RNA q-PCR β2M: F-ATGAGTATGCCTGGCCGTGTGA,	This manuscript	N/A
RNA q-PCR β2M: R-GGCATCTTCAACCTCCATG	This manuscript	N/A
RNA qPCR IL10RA: F- AAGTGGCGCTCCTGAGGTAT	This manuscript	N/A
RNA qPCR IL10RA: R- GCTGTCTGTGCTATTGCTGC	This manuscript	N/A
RNA qPCR TRPS1: F- ACCAGCATGCAGAGTAATATGGT	This manuscript	N/A
RNA qPCR TRPS1: R- GTTCCCTCCCTTACTGGGGC	This manuscript	N/A
RNA qPCR PNRC1:F- CCCCTCAGGAAAGAGGTTT	This manuscript	N/A
RNA qPCR PNRC1: R- TGCCATCAGCTCCCTGTTT	This manuscript	N/A
RNA qPCR CD74: F- TGGCCTTCTGTGGACGAACTC	This manuscript	N/A
RNA qPCR CD74: R- CAGTGACTCTGGAGCAGGTG	This manuscript	N/A
RNA qPCR CD80: F- CCGAGTACAAGAACCGGACC	This manuscript	N/A
RNA qPCR CD80: R- GGTGTAGGAAAGTCAGCTTGA	This manuscript	N/A
PCRCHIP negativeregion:F-GAGGCCAGGGTTCTCTGATT	This manuscript	N/A
PCRCHIP negativeregion:R-CCTCAGTGATCAGCCCTAAATG	This manuscript	N/A
PCR CHIP IL10RA: F- CCCGCTCCATTAAAGTTCTCC	This manuscript	N/A
PCR CHIP IL10RA: R- TTTCAGCCTTCCACTTCC	This manuscript	N/A
PCR CHIP TRPS1: F- AGTTATTTGGAGGGACAGCG	This manuscript	N/A
PCR CHIP TRPS1: R- GTGATTAATGCCTGACAGCG	This manuscript	N/A
PCR CHIP PNRC1:F- GCTGTTTCACTTCTCCCTTG	This manuscript	N/A
PCR CHIP PNRC1: R- AGGATTGTGAGACTTGGGATC	This manuscript	N/A
PCR CHIP CD74:F- CACTTACCAAGCTCCTTCG	This manuscript	N/A
PCR CHIP CD74:R- CTACTTCTGGAGGTGTGATCC	This manuscript	N/A
PCR CHIP CD80:F- TCTACTCCACCTCTGAATCC	This manuscript	N/A
PCR CHIP CD80: R- CTAAAGTCTCCTCATCCCACC	This manuscript	N/A
Software and algorithms		
Thermo Xcalibur Software (v2.4)		
BioRender		
Graphpad		

EXPERIMENTAL MODEL AND STUDY PARTICIPANT DETAILS

Patient details

All children in this cross-sectional study were classified according to the International League Against Rheumatism criteria^{52,53} and divided into three major subgroups: (persistent) oligoarticular JIA, polyarticular JIA (including five extended oligoarticular JIA) and systemic JIA. Blood samples of 16 patients with oligoarticular JIA, 4 patients with polyarticular JIA and 0 patients with systemic

JIA. Among the patients included in our study, 45% were male and 55% were female. Throughout the analysis, we did not observe any differences related to gender. All samples were obtained by the University Medical Center Utrecht, Utrecht, The Netherlands. The study procedures were approved by the Institutional Review Board of the University Medical Center Utrecht (UMCU; METC nr: 11-499c). The study had full ethical approval. Furthermore, synovial fluid samples were obtained at the time of a therapeutic joint aspiration from the same patients. Synovial fluid was collected in sodium heparin tubes and prepared in the same manner as the blood samples. Blood and synovial fluid were centrifuged to remove cells. Cell-free plasma and synovial fluid samples were stored frozen at -80°C until analysis. Table S1 shows the general characteristics of the patients. Informed consent was obtained either from parents or from the individuals directly if they were >12 years. Before each assay, all samples were centrifuged in a polypropylene centrifuge tube containing a 0.22 mm nylon membrane (Spin-X Column; Corning, Corning, New York, USA) to remove debris. Furthermore, the viscosity of the synovial fluid samples was reduced by treatment with hyaluronidase (type IV-S, Sigma-Aldrich, St Louis, Missouri, USA) at a concentration of 20 U/ml for 30 min at 37°C , followed by centrifugation.

Collection of healthy control peripheral blood samples

Peripheral blood (PB) was obtained from healthy donors (HC) under the Minidonor Dienst Program (UMC Hospital) after prior informed consent from each donor. The age range of the donors is unknown, but it is estimated to be between 25 and 60 years old. Additionally, as gender is not disclosed, it is unclear whether the samples were obtained from male or female individuals. PB was drawn at the same moment via vein puncture or intravenous drip. Informed consent was obtained from all patients. The study procedures were approved by the Institutional Review Board of the University Medical Center Utrecht (UMCU; METC nr: 11-499c) and performed according to the principles expressed in the Helsinki Declaration. Synovial fluid mononuclear cells (SFMCs) and peripheral blood mononuclear cells (PBMCs) were isolated using Ficoll Isopaque density gradient centrifugation (GE Healthcare Bio-Sciences AB) and were used fresh or after freezing in FCS (Invitrogen) containing 10% DMSO (Sigma-Aldrich).

METHOD DETAILS

Cell isolation and culture

CD4 $^{+}$ T cells were isolated from SFMCs and PBMCs using MagniSortTM Human CD4 $^{+}$ T cell Enrichment Kit (eBioscience 8804-6811-74). The Cd4 T cells were cultured always in RPMI Medium 1640 + GlutaMAX supplemented with 100 U/ml penicillin, 100 mg/mL streptomycin (all obtained from Life Technologies), and 10% heat-inactivated human AB-positive serum (Invitrogen) at 37°C in 5% CO₂. Where indicated, CD4 T cells were activated with 0.5 $\mu\text{g}/\text{mL}$ plate-bound anti-CD3 (eBioscience; 16-0037) and 0.5 $\mu\text{g}/\text{mL}$ anti-CD28 (eBioscience; 16-0289-85) or with TransAct (5ul/ml, Milteny, 130-111-160) during 12, 24 or 48 h. Where indicated cells were treated with Oligomycin (1 μM Sigma Aldrich), 2DG (50mM Sigma Aldrich), 6,8-Bis(benzylthio) octanoic acid (Sigma Aldrich), 3-(3-Pyridinyl)-1-(4-pyridinyl)-2-propen-1-one (3PO) (25 μM , Sigma-Aldrich SML1343), SB204990 (5 μM , Med Chem Express), BMS303141 (30 μM , Sigma Aldrich), Adalimumab (ADA 10 $\mu\text{g}/\text{mL}$), Entanercept (ENT, 10 $\mu\text{g}/\text{ml}$) Tocilizumab (TCZ 10 $\mu\text{g}/\text{mL}$) or with 30% Synovial Fluid (SF) from patients with JIA.

Chromatin-immunoprecipitation (ChIP)

For each sample, cells were crosslinked with 2% formaldehyde and crosslinking was stopped by adding 0.2 M glycine. Nuclei were isolated in 50 mM Tris (pH 7.5), 150 mM NaCl, 5 mM EDTA, 0.5% NP-40, and 1% Triton X-100 and lysed in 20 mM Tris (pH 7.5), 150 mM NaCl, 2 mM EDTA, 1% NP-40, 0.3% SDS. Lysates were sheared using Covaris microTUBE (duty cycle 20%, intensity 3, 200 cycles per burst, 60-s cycle time, eight cycles) and diluted in 20 mM Tris (pH 8.0), 150 mM NaCl, 2 mM EDTA, 1% X-100. Sheared DNA was incubated overnight with anti-histone H3 acetyl K27 antibody (ab4729; Abcam) pre-coupled to protein A/G magnetic beads. Beads were washed and crosslinking was reversed by adding 1% SDS, 100 mM NaHCO₃, 200 mM NaCl, and 300 mg/mL proteinase K. DNA was purified using ChIP DNA Clean & Concentrator kit (Zymo Research). The Chip DNA was used for sequencing or qPCR.

DNA-RNA-sequencing

End repair, a-tailing, and ligation of sequence adaptors were done using Truseq nano DNA sample preparation kit (Illumina). Samples were PCR amplified, checked for the proper size range, and for the absence of adaptor dimers on a 2% agarose gel, and barcoded libraries were sequenced 75 bp single-end on Illumina NextSeq500 sequencer (Utrecht DNA sequencing facility). Sequencing was performed on an Illumina HiSeq2500 genome analyzer, generating 65 bp single-end reads. The reads were aligned to the Human Reference Genome (hg38), using the genomic aligner bwa (v0.7.17). Duplicate reads were marked using Picard MarkDuplicates (v3.1.1). Peak calling over input control was carried out using the MACS3 (v3.0.1) peak caller using narrowPeaks, followed by the generation of consensus peak lists using MSPC (v6.0.0). Bigwig files (RPGC normalization) and tornado plots were created by DeepTools (v3.5.5). Further visualization was accomplished in R with DiffBind (v3.14.0) for finding differentially expressed peaks and ChipSeeker (v1.40.0) for annotation of the peaks. DiffBind performs robust normalization of the data, which helps account for differences in library size and composition between samples. This normalization step is crucial for distinguishing between global shifts in H3K27Ac levels and specific regulatory changes at individual loci. The default TMM (Trimmed Mean of M-values) normalization method was used. Differential peaks between JIA and HC samples were identified using DiffBind (v3.14.0), with significance

thresholds set at FDR <0.05 and log fold change (± 1.5). Filtered peak tables were then reformatted for input into HOMER (v4.11) for motif analysis. Transcription factor word clouds were generated using the wordcloud package (v1.9.3), where font size corresponds to log p -value, with larger fonts indicating higher significance. The top 10 transcription factor families, ranked by absolute significance, are highlighted in distinct colors, while remaining families are grouped under "Other."

Total cellular RNA was extracted using the RNAeasy kit (QIAGEN). Sample preparation was performed using TruSeq stranded total RNA with ribo-zero globin sample preparation kit (Illumina), and samples were sequenced 75 bp single-end on Illumina NextSeq500 (Utrecht DNA sequencing facility).

ChIP-qPCR

Real-time PCR was performed with PowerSYBR (Applied Biosystems) using a StepOnePlus Real-Time PCR system (Applied Biosystems). The expression of each gene was normalized to a negative region. All the primers for the ChIP-qPCR they were designed based on or Chip-seq: qPCR CHIP negative region: F- GAGCCAGGGTTCTGATT, R- CCTCAGTGATCAGCCCTAAATG; qPCR CHIP IL10RA(Promotor Region): F- CCCGCTCCATTAAAGTTCTCC, R- TTTCAGCCTCTTCACTTCC; qPCR CHIP TRPS1 (Promotor Region): F- AGTTATTGGAGGGACAGCG, R- GTGATTAATGCCTGACAGCG; qPCR CHIP PNRC1:(Promotor Region) F- GCTTCTTCACTTCTCCCTTG, R- AGGATTGTGAGACTTGGGATC; qPCR CHIP CD74 (Promotor Region): F- CACTTACCAAGCTCTCTCG, R- CTACTTCTGGAGGTGTGATCC and qPCR CHIP CD80 (Promotor Region): F- TCTACTCCCACCTCTGAATCC, R- CTAAAGTCTTCATCCCACC.

Real-Time PCR

RNA was isolated from cells using RNasy Mini Kit (Qiagen) and cDNA was synthesized using Superscript-III First-Strand Synthesis System (Life Technologies). Real-time PCR was performed with PowerSYBR (Applied Biosystems) using a StepOnePlus Real-Time PCR system (Applied Biosystems). Expression of each gene was normalized to β 2M. The following primer sets were used: RNA q-PCR β 2M: F- ATGAGTATGCCCTGGCCGTGTGA, R- GGCATCTCAAACCTCCATG; RNA qPCR IL10RA: F- AAGTGGCGCTCCTGAGGTAT, R- GCTGCTGTGCTATTGCTGC; RNA qPCR TRPS1: F- ACCAGCATGCAGAGTAATATGGT, R- GTTCCCTCCCTACTGGGC; RNA qPCR PNRC1: F- CCCCCTCAGGAAAGAGGTTTT, R- TGCCATCAGCTCCCTGTTTT; RNA qPCR CD74: F- TGGCCTTCTGTGGACGAATC, R- CAGTGACTCTGGAGCAGGTG; RNA qPCR CD80: F- CCGAGTACAAGAACCGGACC, R- GGTGTAGGGAA GTCAGCTTGA.

Seahorse assays

T cells were stimulated with anti-CD3 and anti-CD28 for 12, 24, and 48 h. Oxygen consumption rates (OCR) and extracellular acidification rates (ECAR) were measured in XF media (non-buffered RPMI 1640 containing 10 mM glucose, 2 mM L-glutamine, and 1 mM sodium pyruvate) under basal conditions and in response to glucose 30mM, 1uM oligomycin, and 50mM of 2DG, on an XF-24 Extracellular Flux Analyzers (Seahorse Bioscience).

Measurements of acetyl-CoA levels

The intracellular levels of acetyl-CoA were detected by using an Acetyl-CoA Assay Kit (Biovision, Milpitas CA), following the manufacturer's instructions.

Sample preparation and LC-MS measurement of glycolytic/TCA cycle intermediates

Polar metabolites were extracted from 2x10⁶ T-cells isolated from peripheral blood or synovial fluid by adding 500 μ L ice-cold methanol solution containing internal standards. The cell lysis was performed by using a bullet blender and 0.5 mm glass beads (NextAdvance, USA) in the sample tube. After cell lysis the extracts were centrifuged for 10 min at 17000xg and 4°C. The complete supernatant was transferred into a fresh 1.5mL tube and evaporated to dryness in a vacuum concentrator (Labconco CentriVap, USA) for 1h. The dried metabolite pellet was dissolved in 120 μ L of water/acetonitrile solution (95%/5%, v/v) prior to transfer the material into LC glass vials.

The chromatographic separation was performed using a ThermoFischer Accela UHPLC System equipped with a Waters Acuity C8 column (2.1 x 150 mm, 1.8 μ m) the outlet of which was connected to an LTQ-Orbitrap XL MS System (ThermoFisher Scientific, USA and Waters, USA). The LC flow rate was set to 150 μ L/min and the column oven temperature was adjusted to 35°C. Five microliters of the sample was injected on column. The weak and the strong eluents were 100% Milli-Q water and methanol/Milli-Q water (95%/5%, v/v) respectively and both solvents contain 6.5mM ammonium bicarbonate at pH 8.0. The strong eluent starts at 0% for 1min and increases over 1-5min from 0% to 70% and from 70% to 98% between 5 and 5.5min following an isocratic run over 5.5–15.5min and a drop back to the initial 0% composition between 15.5 and 22min. The MS data were acquired in full scan mode between 55 and 900 amu. The peak picking and integration was performed with Thermo Xcalibur Software (v2.4). The target metabolites were identified by running authenticated standards in parallel and comparing their retention time and m/z values. The obtained peak areas were corrected by the peak area of the corresponding internal standard.

QUANTIFICATION AND STATISTICAL ANALYSIS**Statistical analysis**

For ChIP-seq and RNA-seq analysis, p values were adjusted with the Benjamini-Hochberg procedure. For ChIP-seq regions with a significantly different H3K27ac signal were defined using a false discovery rate (FDR) < 0.05 .

Data are presented as the mean \pm SEM, with a minimum of $n = 3$ per group. Each data point shown in the graphs represents an independent experiment. For additional details, please refer to the Figure Legends. p values were calculated using the unpaired Student's t test, or one or two-way ANOVA using and Tukey test correction for multiple comparisons. The graphs and statistical analyses were generated using Prism 9.3.1 (GraphPad). Statistical significance was set at $p \leq 0.05$, with levels indicated by asterisks as follows: * $p \leq 0.05$; ** $p \leq 0.01$; *** $p \leq 0.001$; **** $p \leq 0.0001$; ns, not significant.